Scripta Materialia 186 (2020) 242–246

Contents lists available at ScienceDirect

Scripta Materialia

journal homepage: www.elsevier.com/locate/scriptamat

Development of Ti–Zr–Hf–Y–La high-entropy alloys with dual hexagonal-close-packed structure

Takeshi Nagase[a,b], Mitsuharu Todai[c], Takayoshi Nakano[b,*]

[a] Research Center for Ultra-High Voltage Electron Microscopy, Osaka University, 7-1, Mihogaoka, Ibaraki, Osaka 567-0047, Japan
[b] Division of Materials and Manufacturing Science, Graduate School of Engineering, Osaka University, 2-1, Yamadaoka, Suia, Osaka 565-0871, Japan
[c] Department of Environmental Materials Engineering, National Institute of Technology, Niihama College, 7-1 Yagumo-cho Niihama, Ehime 792-8580, Japan

ARTICLE INFO

Article history:
Received 13 March 2020
Revised 21 April 2020
Accepted 13 May 2020
Available online 5 June 2020

Keywords:
High entropy alloys
Metals and alloys
Microstructure
Solidification
Liquid phase separation
Biomaterials

ABSTRACT

$TiZrHfYLa_{0.2}$ high-entropy alloys (HEAs) with dual hexagonal-closed-packed (HCP) structures were designed based on the concept of liquid phase separation (LPS) and segregation for enhancing the immiscibility of the constituent elements. The LPS leads to a particular solidification microstructure on the free surface side and Cu-hearth contacted area in the ingots. The dual HCP structures with equi-axis Ti–Zr–Hf dendrite and Y-La-rich interdendrite were observed at most regions of the arc-melted ingots. The mixing enthalpy among the constituent elements and predicted phase diagrams constructed by the Materials Project were effective for the alloy design of the HEAs with dual HCP structures.

A new generation of structural and functional materials are urgently required to meet the Sustainable Development Goals (SDGs). Recently, a new class of structural and biomedical materials called high-entropy alloys (HEAs) including HEAs for metallic biomaterials (bio-HEAs) was developed [1–16]. Various alloy definitions of HEAs were suggested [8,9], and the entropy-based definition of $\Delta S_{mix} \geq 1.5R$ was used in the present study, where ΔS_{mix} was the mixing entropy of the ideal and regular solutions in the alloys and R was the gas constant. Most structures in the solid solution phases in HEAs were body-centered-cubic (BCC) or face-centered-cubic (FCC) structures [8,9]. The hexagonal-close-packed (HCP) structure formation was strictly limited. To clarify the origin of single HCP and dual HCP phases formation via high-entropy scheme is important for the construction of the alloy design theory of HEAs. Focusing on the formation of the HCP phase as the main constituent phases in the ingots without thermomechanical treatment, only a few alloy systems were reported to date: the rare-earth-based alloys of Y–Gd–Tb–Dy–Lu [17], Gd–Tb–Dy–Tm–Lu [17], Ho–Dy–Y–Gd–Tb [18], the combination of refractory HEAs (RHEAs) and the rare-earth based alloys of Ti–Zr–Hh–*Sc*–Y–La with dual HCP [19] and Ti–Zr–Hf–Al–*Sc* [20], precious-metal-based HEAs of Ir–Mo–Rh–Ru–W [21,22], 3*d* transition metal type (3*d*-HEAs) of Co–Cr–Mo–Fe–Mn–W [23], and Co–Cr–Mo–Fe–Mn–W–Ag [23]. It should be emphasized here that the present study focused on the HCP phase formation in the ingots, not on the formation of the HCP phase under high-pressure conditions such as Co–Cr–Fe–Mn–Ni HEA [24], by mechanical milling such as Al–Ti–Mg–Li–*Sc* [25], by chemical reaction such as Ir–Os–*Re*–Rh–Ru [26], that at the solid state phase transition by thermomechanical treatment such as 3*d*-HEAs of Co–Cr–Fe–Mn–Ni [27–29], and RHEAs in Hf–Nb–Ta–Ti–Zr [30–32] and Ti–Nb–Ta–Zr–Al [33]. Some of reports [27–30], 32] among above-described papers reported that the formation of the HCP phase was effective to modify the mechanical strength and/or ductility in HEAs. The research that focused on single HCP and/or dual HCP phases formation is important for clarifying not only the origin of solid-solution formation behavior in HEAs but also the structural control of HEAs for modifying the mechanical properties. This paper describes the formation of dual-HCP structure in the arc-melted ingots in Ti–Zr–Hf–Y–La HEAs, which was designed based on the concept of the immiscibility of constituent elements via liquid phase separation (LPS) and segregation during the solidification. The alloy design of HEAs with dual HCP phases via LPS and/or segregation was as follows: (1) LPS-type HEAs with dual HCP structures; the LPS of thermal melt leads to the formation of the separated liquid phases, and both the separated liquids transform each other into HCP phases, resulting in the formation of the dual HCP structure. (2) Segregation-related HEAs with dual HCP structures; the formation of the primary HCP phase during solidification leads to the formation of the composite of the primary

* Corresponding author.
E-mail address: nakano@mat.eng.osaka-u.ac.jp (T. Nakano).

https://doi.org/10.1016/j.scriptamat.2020.05.033

(a) $\Delta H_{i\text{-}j}$ [kJ/mol]

	Ti	Zr	Hf	Y	La
Ti		0	0	15	20
Zr			0	9	13
Hf				11	15
Y					0
La					

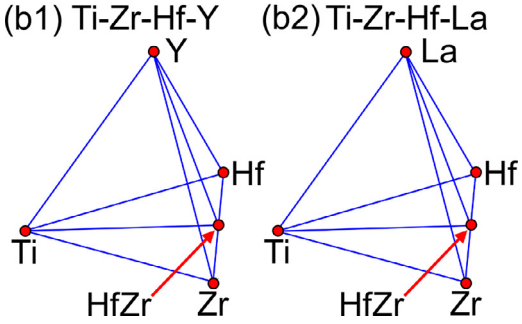

Fig. 1. Alloy prediction for liquid phase separation in Ti–Zr–Hf–Y–La alloy system. (a) $\Delta H_{i\text{-}j}$ map among Ti, Zr, Hf, Y, and La. (b1) Predicted phase diagram of Ti–Zr–Hf–Y. (b2) Predicted phase diagram of Ti–Zr–Hf–La.

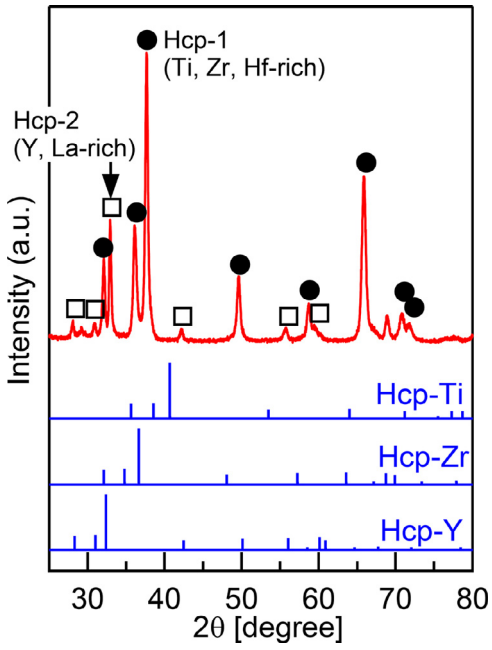

Fig. 2. XRD pattern of central region of arc-melted ingots in $TiZrHfYLa_{0.2}$ alloy.

HCP solid and residual liquid; thereafter, the residual liquid transforms into the secondary HCP phase, resulting in dual HCP phases. The LPS and segregation in alloys are connected—LPS behavior in alloys is closely related to that of flat liquidus in the phase diagram, and the flat liquidus leads to a high degree of segregation during solidification. It should be noted here that the concept of eutectic HEAs (EHEAs) was suggested concerning the development of dual-phase HEAs via the melting and solidification processes; the eutectic reaction of the thermal melt resulted in the formation of dual-phase HEAs with fine lamella structures [34,35]. The present study for the formation of dual-phase HEAs with HCP structures via the melting and solidification process focuses not on the eutectic reaction but on the LPS and segregation. The LPS in HEAs was reported in various alloy systems: Al–Co–Cr–Cu–Ni–Ag [36], Al–Cr–Cu–Fe–Ni [37,38], Co–Ni–Cu–Al–Cr [39], Co–Cr–Cu–Fe–Mo–Ni [40], Co–Cr–Cu–Fe–Ni [41–44], Cr–Cu–Fe–Mo–Ni [45], Co–Cu–Fe HEAs with the addition of Al, Cr, Mn, Ni, V, or Ti [46], Co–Cr–Cu–Fe–Ni–Sn [47], Co–Cr–Fe–Mn–Ni–Ag [48], Al–Cr–Fe–Ni–Mo [49], and Co–Cr–Mo–Fe–Mn–W–Ag [23]. The review paper for the LPS in HEAs [50] concluded that the LPS was a general phenomenon in HEAs. The Ti–Zr–Hf–Y–La HEAs were designed for the formation of the Ti–Zr–Hf-rich liquid and La–Y-rich liquid via LPS and segregation and the formation of the dual-phase HEAs with Ti–Zr–Hf-rich and La–Y-rich phases. The LPS behavior during melting and solidification in the Ti-based alloys was reported in some alloy systems of Ti-rare earth elements: Ti–La- [51,52], Ti–Ce- [52], Ti–Nd- [52], and Ti–Ag-based alloy system of Ti–Ag [53] and Ti–Ag–Nb [54]. Based on the above-described reports, the Ti–Zr–Hf–Y–La alloy system was considered.

For the design technique of multicomponent alloys with LPS, the combination of the mixing enthalpy of the *i, j* element pairs ($\Delta H_{i\text{-}j}$) and the predicted phase diagram used by the Materials Project [55,56] was clarified to be effective in the various alloy systems of Fe–Cu–Nb–B [57], Fe–Cu–Si–B [58,59], Fe–Cu–Zr–B [58,59], Fe–Ag–Si–B [59,60], Fe–Sn–Si–B [60], Co–Cu–Zr–B [61], Al–Co–La–Pb [62], and Cu–Ag–La–Fe [63]. Fig. 1 shows the alloy prediction for the LPS tendency in the Ti–Zr–Hf–Y–La alloy system by the matrix of $\Delta H_{i\text{-}j}$ (Fig. 1a) and the predicted phase diagram using the Materials Project (Fig. 1b1, 1b2). The value of $\Delta H_{i\text{-}j}$ was obtained from the literature [64]. The value of $\Delta H_{i\text{-}j}$ for Ti, Zr, and Hf was 0, whereas its value for i = Ti, Zr, Hf; j = *Y* and i = Ti, Zr, Hf; j = La was large and positive; $\Delta H_{i\text{-}j} \geq +10$ kJ/mol. The value of $\Delta H_{i\text{-}j}$ (i = La; j = *Y*) was 0. The matrix of $\Delta H_{i\text{-}j}$ in Ti–Zr–Hf–Y–La indicates the tendency for the LPS to form Ti–Zr–Hf- and Y-La-rich liquids. In the predicted phase diagrams of Ti–Zr–Hf–Y (Fig. 1b1) and Ti–Zr–Hf–La (Fig. 1b2), HfZr compounds [65] are displayed with ordered HCP structures. The formation energy of HfZr was significantly small with a value of −0.096 kJ/mol, indicating that the formation of HfZr at ambient temperature is distant. No binary (i = Ti, Zr, Hf; j = *Y*, La), ternary (*i, j* = Ti, Zr, Hf; k = *Y*, La), and quaternary (Ti–Zr–H–*X*; *X* = *Y*, La) compounds were identified in the predicted phase diagrams (Fig. 1b1, 1b2). This indicates that the LPS for the Ti–Zr–Hf- and Y–La-rich liquid formation is not prevented by the intermetallic compound formation during the cooling of the thermal melt. Based on the alloy prediction for the LPS in the Ti–Zr–Hf–Y–La alloy system, $TiZrHfYLa_{0.2}$, for which $\Delta S_{mix} = 1.5R$ was designated, and the solidification microstructure of the ingots in the $TiZrHfYLa_{0.2}$ alloy were investigated, focusing on the formation of the HCP phase and the elemental distribution.

Arc-melted ingots of the $TiZrHfYLa_{0.2}$ alloy were prepared by mixing lumps of the pure elements. The purity of the Ti and Zr resources was above 3 N (99.9%) and that of the Hf, Y, and La rumps was above 2 N. The cooling rate during the solidification in the arc-melting process was estimated experimentally as approximately 2000 K/s [53,66]; its values were estimated by the secondary dendrite arm spacing in the Al-Cu alloys experimentally. The cooling rate during the arc-melting process was an order higher than the metallic mold casting [67] and three orders higher than the silica-based crucible cooling of the thermal melt [68]. The microstructure and constituent phases of the ingots and annealed specimens were investigated using X-ray diffraction (XRD) analysis, scanning electron microscopy (SEM), and electron probe microanalysis (EPMA).

Fig. 2 depicts the XRD pattern of the central region of the arc-melted ingots in the $TiZrHfYLa_{0.2}$ alloy together with the calculated X-ray intensity of the HCP phases of Ti [69], Zr [70], and Y [71]. The peak position and intensity of the X-ray diffraction of the HCP

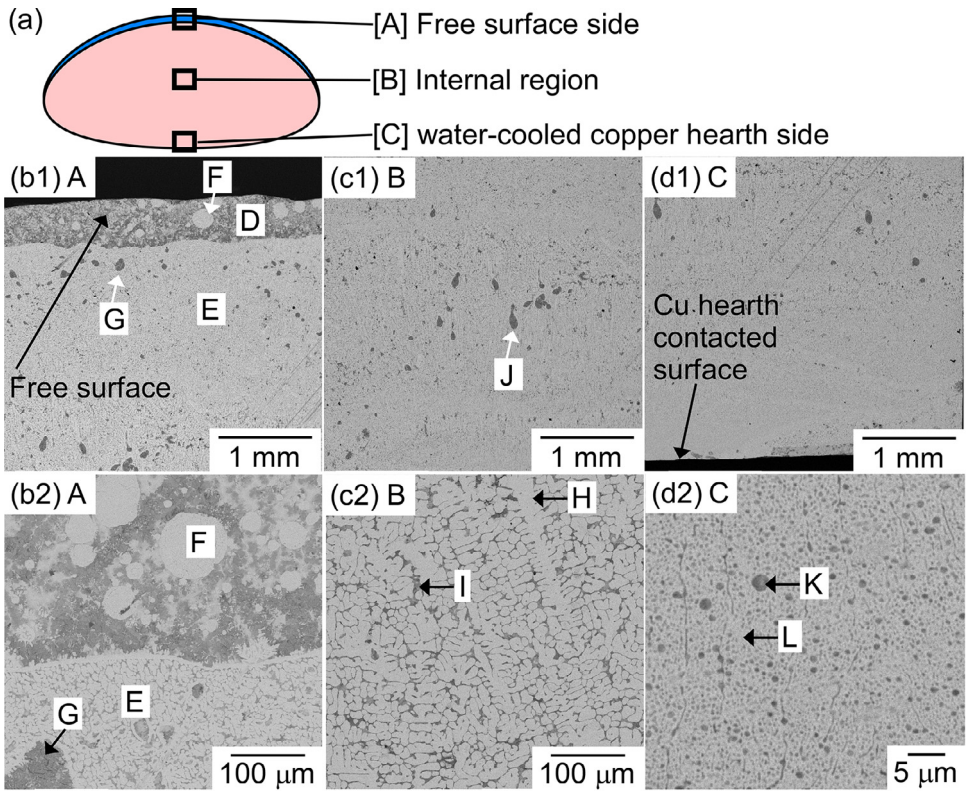

Fig. 3. Solidification microstructure of arc-melted ingot in $TiZrHfYLa_{0.2}$ alloy. (a) Schematic of cross section of ingot focusing on solidification microstructure, SEM-BSE images of (b1) & (b2) free surface side [A], (c1) & (c2) internal region [B], (d1) & (d2) Cu hearth contacted surface side [C]. (b2), (c2), and (d2) are magnified images of (b1), (c1), and (d1), respectively.

phases in Hf and La were similar to those in Zr and Y, respectively. The sharp peaks in XRD pattern can be indexed as dual HCP phases indicated by the closed-circles (●) and open squares (□). The peaks indicated by ● and □ were considered Ti–Zr–Hf-based and Y–La-based HCP phases according to the positions of the peaks in the XRD patterns together with the solidification analysis results presented in the latter parts.

Fig. 3 shows the solidification microstructure analysis results of the arc-melted ingot in the $TiZrHfYLa_{0.2}$ alloy obtained from SEM–back scattering electron (BSE) images. Fig. 3a presents a schematic of the cross section of the ingots. The macroscopically heterogeneous microstructures were observed in the ingots, and the microstructure can be classified into three regions: (1) Index A, macroscopically phase-separated structure at the free surface side, as depicted in Figs. 3b1 and 3b2. (2) Index B, equi-axis dendrite region with globules at the internal region depicted in Figs. 3c1 and 3c2. (3) Index C, fine emulsion-type solidification microstructure at the Cu hearth contacted region, as displayed in Figs. 3b1 and 3d2. The solidification microstructure indicated by indexes A and C was minor, and most of the region in the arc-melted ingots displayed the equi-axis dendrite structure, indicated by index B. The free surface side region (Figs. 3b1 and 3b2) illustrates the macroscopically phase-separated structure with the gray contrast surface layer (D) and white contrast matrix region (E). The white contrast globules (F) were embedded in the surface gray contrast layer (D), whereas the gray contrast globules (G) were embedded in the white contrast matrix (E) at the internal region. At the central region, the equi-axis dendrite region composed of the white contrast dendrite (H) and gray contrast interdendrite region (I) was observed. The gray contrast globules (J) with a small area fraction were embedded in the equi-axis dendrite matrix. The emulsion-like structure composed of fine gray contrast globules (K) embedded in the white contrast matrix (L) was seen at the Cu hearth contacted region in Figs. 3c1 and 3c2. The significant difference in the contrast was not observed in the SEM-BSE images of the gray contrast region among the regions D and G in Figs. 3b1 and 3b2, I and J in Fig. 3c1 and 3c2, and K in Fig. 3d2. The significant difference in the contrast was also not observed in the SEM-BSE images of the white contrast region among the regions E and F in Figs. 3b1 and 3b2, H in Fig. 3c1, and L in Fig. 3d2.

Fig. 4 presents the EPMA–wave dispersive spectroscopy (WDS) analysis results of the arc-melted ingot in the $TiZrHfYLa_{0.2}$ alloy, focusing on the regions A and B in Fig. 3. The EPMA-WDS analysis in the region C, as depicted in Fig. 3, was not applicable because of the lack of spatial resolution in EPMA with the W filament thermionic-emission electron gun used in the present study. In the region A of the free surface side (Fig. 4a), a macroscopically phase-separated structure composed of Y-La- (corresponding to the region D depicted in Fig. 3) and Ti–Zr–Hf-rich regions (corresponding to the region E depicted in Fig. 3, hereafter referred to as “E in Fig. 3”) was observed. The Ti–Zr–La-rich globules (F in Fig. 3), embedded in the Y–La-rich matrix (D in Fig. 3), and Y–La-rich globules (G in Fig. 3), embedded in the Ti–Zr–Hf-rich region (E in Fig. 3), were also observed. In the internal region (Fig. 4b1), Ti–Zr–Hf-rich dendrite (H in Fig. 3) and Y–La-rich interdendrite (I in Fig. 3) were observed. Figs. 4b2 and 4b3 present the quantitative chemical composition analysis results at the dendrite (H in Fig. 3) and interdendrite (I in Fig. 3) regions, respectively. The solubilities of Y and La in the dendrite region (H in Fig. 3) were significantly small. This indicates that Y and La were rejected from the dendrite (H in Fig. 3) and enriched in the residual liquid, resulting in the formation of the Y–La-rich interdendrite phase (I in Fig. 3).

The macroscopically phase-separated structure at the free surface side depicted in Figs. 3b1, 3b2, and 4 was characterized by

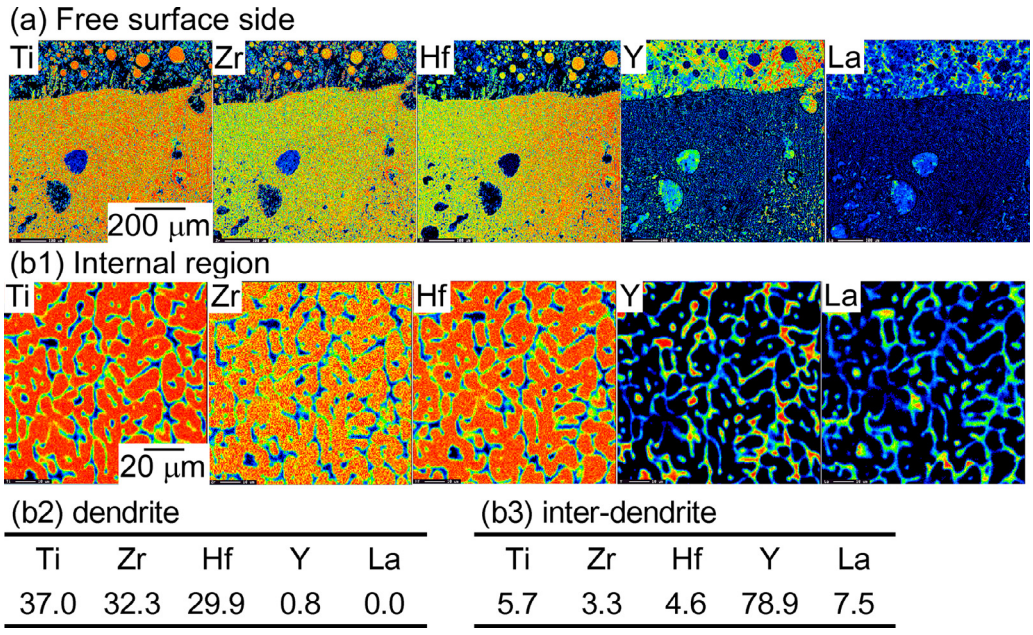

(b2) dendrite

Ti	Zr	Hf	Y	La
37.0	32.3	29.9	0.8	0.0

(b3) inter-dendrite

Ti	Zr	Hf	Y	La
5.7	3.3	4.6	78.9	7.5

Fig. 4. EPMA-WDS analysis results of arc-melted ingot in $TiZrHfYLa_{0.2}$ alloy. (a) elemental mapping of free surface side [A] focusing on macroscopically phase-separated region; (b) elemental mapping of internal region focusing on dendrite and inter-dendrite regions [B]. (c) Composition analysis of dendrite and interdendrite regions at internal region [B].

the smooth interface at the Ti–Zr–Hf-rich and Y–La-rich regions and the globules. The emulsion-like structure was observed in the Cu-hearth contacted side, as depicted in Figs. 3d1 and 3d2, and the gray contrast globules and white contrast matrix were considered to correspond to the Y–La-rich fine globules and Ti–Zr–Hf-rich matrix, respectively. These phase-separated structures and emulsion-like structures were typical for the alloys with LPS. At the central region depicted in Figs. 3b1, 3b2, and 4b1, the segregation led to the formation of a Ti–Zr–Hf-rich dendrite with HCP structure and a Y–La-rich interdendrite with HCP structure. It was reasonable to consider that the rejection of Y and La forming Ti–Zr–Hf-rich dendrites during the solidification corresponded to the repulsive characteristics between the Ti–Zr–Hf and Y–La elements depicted in Fig. 1a. The alloy design based on the positive values in $\Delta H_{i\text{-}j}$ and the suppression of the intermetallic compound formation was effective to form the chemical element separated phase via LPS and the high degree of segregation during the cooling of the thermal melt in multicomponent alloys, resulting in dual-phase HEAs. The mechanical properties of HEAs and the effect of HCP phase formation on the mechanical properties were the important topics in HEAs. The Micro-Vickers hardness (*Hv*) test was performed with a load setting of 1.0 kgf, where *Hv* was evaluated using the average value and standard deviation (Std.) of 10 measured pieces of data. The *Hv* in the internal region (B in Fig. 3) was 268 (Std. 14.4), and that in the water-cooled copper-contacted hearth region (C in Fig. 3) was 271 (Std. 9.5). No significant difference in *Hv* between the central and bottom regions in the ingots was observed. The compressive and/or tensile tests were not performed, and these will be reported in the other literatures. The dual HCP phase formation in the arc-melted ingot in the $TiZrHfYLa_{0.2}$ alloy was achieved by the alloy design with positive $\Delta H_{i\text{-}j}$ among constituent elements. The alloy design in HEAs with positive $\Delta H_{i\text{-}j}$ among constituent elements was reported to be effective for achieving moderate ductility and high mechanical strength in Co–Cr–Cu–Fe–Ni HEAs with liquid-phase separation [43] and Co–Cr–Cu–Mn–Ni HEAs [72,73]. These reports indicate the importance of the alloy design in HEAs with positive $\Delta H_{i\text{-}j}$ among constituent elements.

In conclusion, $TiZrHfYLa_{0.2}$ HEAs with dual-HCP structures were designed based on the concept of the LPS and segregation for enhancing the immiscibility of the constituent elements. The LPS leads to a particular solidification microstructure on the free surface side and Cu hearth contacted area in the ingots. The dual-HCP structure with equi-axis Ti–Zr–Hf dendrite and Y–La-rich interdendrite was observed at most regions of the arc-melted ingots. The $\Delta H_{i\text{-}j}$ matrix and predicted phase diagrams obtained by the Materials Project was effective for the design of the dual-phase HEAs with LPS and segregation.

Declaration of Competing Interests

The authors declare that they have no known competing financial interests or personal relationships that could have appeared to influence the work reported in this paper.

Acknowledgments

This work was partially supported by KAKENHI (Grant Number 18H05254, 18K04750, and 19H05172), the Council for Science, Technology and Innovation (CSTI), Cross-Ministerial Strategic Innovation Promotion Program (SIP), and Innovative Design/Manufacturing Technologies program (Establishment and Validation of the base for 3D Design & Additive Manufacturing Standing on the Concepts of “Anisotropy” & “Customization”) of the New Energy and Industrial Technology Development Organization (NEDO).

Authors contributions

T. Nagase: Investigation, original draft
M. Todai: Investigation
T. Nakano: Supervision, review and edit

Supplementary materials

Supplementary material associated with this article can be found, in the online version, at doi:10.1016/j.scriptamat.2020.05.033.

References

[1] B. Cantor, I.T.H. Chang, P. Knight, A.J.B. Vincent, Mater. Sci. Eng. A 375-377 (2004) 213–218 https://doi.org/10.1016/j.msea.2003.10.257.
[2] J.W. Yeh, S.K. Chen, S.J. Lin, J.Y. Gan, T.S. Chin, T.T. Shun, C.H. Tsau, S.Y. Chang, Adv. Eng. Mater. 6 (2004) 299–303 https://doi.org/10.1002/adem.200300567.
[3] S. Ranganathan, Curr. Sci. 85 (2003) 1404–1406 https://www.currentscience.ac.in/Downloads/article_id_085_10_1404_1406_0.pdf.
[4] Y. Zhang, Y.J. Zhou, J.P. Lin, G.L. Chen, P.K. Liew, Adv. Eng. Mater. 10 (2008) 534–538 https://doi.org/10.1002/adem.200700240.
[5] J.W. Yeh, JOM 65 (2013) 1759–1771 https://doi.org/10.1007/s11837-013-0761-6.
[6] M.H. Tsai, J.W. Yeh, Mater. Res. Lett. 2 (2014) 107–123 https://doi.org/10.1080/21663831.2014.912690.
[7] Y. Zhang, T.T. Zuo, Z. Tang, M.C. Gao, K.A. Dahmen, P.K. Liaw, Z.P. Lu, Prog. Mater. Sci. 61 (2014) 1–93 https://doi.org/10.1016/j.pmatsci.2013.10.001.
[8] B.S. Murty, J.-.W. Yeh, S. Ranganathan, High-Entropy Alloys, 1st ed., Elsevier, 2014.
[9] M.C. Gao, J.-.W. Yeh, P.K. Liaw, Y. Zhang, High-Entropy Alloys, Fundamentals and Applications, 1st ed., Springer, 2016.
[10] A. Takeuchi, J. Jpn. Inst. Metal. 79 (2015) 157–168 https://doi.org/10.2320/jinstmet.J2014046.
[11] A. Takechi, J. Jpn, Soc, Powder. Metall. 63 (2016) 209–216 https://doi.org/10.2497/jjspm.63.209.
[12] Y.F. Ye, Q. Wang, J. Lu, C.T. Liu, Y. Yang, Materials Today 19 (2016) 349–362 https://doi.org/10.1016/j.mattod.2015.11.026.
[13] D.B. Miracle, O.N. Senkov, Acta Mater. 122 (2017) 448–511 https://doi.org/10.1016/j.actamat.2016.08.081.
[14] T. Nagase, J. Soc. Mech. Eng. 121 (1192) (2018) 8–11 https://doi.org/10.1299/jsmemag.121.1192_8.
[15] W. Zhang, P.K. Liew, Y. Zhang, Sci. China Mater. 61 (2018) 2–22 https://doi.org/10.1007/s40843-017-9195-8.
[16] D.B. Miracle, Nat. Commun. 10 (2019) 1805 https://doi.org/10.1038/s41467-019-09700-1.
[17] A. Takeuchi, K. Amiya, T. Wada, K. Yubuta, W. Zhang, JOM 66 (2014) 1984-1192 https://doi.org/10.1007/s11837-014-1085-x .
[18] M. Feuerbacher, M. Heidelmann, C. Thomas, Mater. Res. Lett. 3 (2015) 1–6 http://doi.org/10.1080/21663831.2014.951493.
[19] A. Takeuchi, Intermetallics 69 (2016) 103–109 https://doi.org/10.1016/j.intermet.2015.10.022.
[20] L. Rogal, P. Bobrowski, F. Kormann, S. Divinski, F. Stein, B. Grabowski, Sci. Rep. 7 (2016) 2209 http://doi.org/10.1038/s41598-017-02385-w.
[21] A. Takeuchi, T. Wada, H. Kato, Mater. Trans. 60 (2019) 1666–1673 https://doi.org/10.2320/matertrans.M2019037.
[22] A. Takeuchi, T. Wada, H. Kato, Mater. Trans. 60 (2019) 2267–2276 https://doi.org/10.2320/matertrans.MT-M2019212.
[23] T. Nagase, M. Todai, T. Nakano, Mater. Trans. 61 (2020) 567–576 https://doi.org/10.2320/matertrans.MT-MK2019002.
[24] C.L. Tracy, S. Park, D.R. Rittman, S.J. Zinkle, H. Bei, M. Lang, R.C. Ewing, W.L. Mao, Nat. Commun. 8 (15) (2017) 634 https://doi.org/10.1038/ncomms15634.
[25] K.M. Youssef, A.J. Zaddach, C. Niu, D.L. Irving, C.C. Koch, Mater. Res. Lett. 3 (2015) 95–99 https://doi.org/10.1080/21663831.2014.985855.
[26] K.V. Yusenko, S. Riva, P.A. Carvalho, M.V. Yusenko, S. Arnaboldi, A.S. Sulthikh, M. Hanfland, S.A. Gromilov, Scr. Mater. 138 (2017) 22–27 https://doi.org/10.1016/j.scriptamat.2017.05.022.
[27] Z. Li, K.G. Pradeep, Y. Deng, D. Raabe, C.C. Tasan, Nature 534 (2016) 227–230 https://doi.org/10.1038/nature17981.
[28] Z. Li, F. Kormann, B. Grabowski, J. Neugebauer, D. Raabe, Acta Mater. 136 (2017) 262–270 https://doi.org/10.1016/j.actamat.2017.07.023.
[29] D. Wei, X. Li, J. Jiang, W. Heng, Y. Koizumi, W.-.M. Choi, B.-.J. Lee, H.S. Kim, H. Kato, A. Chiba, Scr. Mater. 165 (2019) 39–43 https://doi.org/10.1016/j.scriptamat.2019.02.018.
[30] N.D. Stepanov, N.Yu Yurchenko, S.V. Zherebtsov, M.A. Tikhonovsky, G.A. Salishchev, Mater. Lett. 211 (2018) 87–90 https://doi.org/10.1016/j.matlet.2017.09.094.
[31] S.Y. Chen, Y. Tong, K.-.K. Tseng, J.-.W. Yeh, J.D. Poplawsky, J.G. Wen, M.C. Gao, G. Kim, W. Chen, Y. Ren, R. Feng, W.D. Li, P.K. Liaw, Scr. Mater. 158 (2019) 50–56 https://doi.org/10.1016/j.scriptamat.2018.08.032.
[32] C. Yang, K. Aoyagi, H. Bian, A. Chiba, Mater. Lett. 254 (2019) 46–49 https://doi.org/10.1016/j.matlet.2019.07.027.
[33] Y. Cao, Y. Liu, Y. Li, B. Liu, A. Fu, Y. Nie, Int. J. Refract. Met. Hard Mater. 86 (2020) 105 132 https://doi.org/10.1016/j.ijrmhm.2019.105132 .
[34] Y. Lu, Y. Dong, S. Guo, L. Jiang, H. Kang, T. Wang, B. Wen, Z. Wang, J. Jie, Z. Cao, H. Ruan, T. Li, Sci. Rep. 4 (2014) 06200 1-5 https://doi.org/10.1038/srep06200 .
[35] Y. Lu, X. Gao, L. Jiang, Z. Chen, T. Wang, J. Jie, H. Kang, Y. Zhang, S. Guo, H. Ruan, Y. Zhao, Z. Cao, T. Li, Acta Mater. 124 (2017) 143–150 https://doi.org/10.1016/j.actamat.2016.11.016.
[36] U.S. Hsu, U.D. Hung, J.W. Yeh, S.K. Chen, Y.S. Huang, C.C. Yang, Mater. Sci. Eng., A 460-461 (2007) 403–408 https://doi.org/10.1016/j.msea.2007.01.122.
[37] S. Guo, C. Ng, C.T. Liu, J. Alloys Compd. 557 (2013) 77–81 https://doi.org/10.1016/j.jallcom.2013.01.007.
[38] A. Munitz, S. Samuha, E. Brosh, S. Salhov, N. Derimow, R. Abbaschian, Intermetallics 97 (2018) 77–84 https://doi.org/10.1016/j.intermet.2018.04.004.
[39] A. Munitz, M.J. Kaufman, J.P. Chandler, H. Kalaantari, R. Abbaschian, Mater. Sci. Eng., A 560 (2013) 633–642 https://doi.org/10.1016/j.msea.2012.10.007.
[40] P.H. Wu, N. Liu, W. Yang, Z.X. Zhu, Y.P. Lu, X.J. Wang, Mater. Sci. Eng. A 642 (2015) 142–149 https://doi.org/10.1016/j.msea.2015.06.061.
[41] N. Liu, P.H. Wu, P.J. Zhou, Z. Peng, X.J. Wang, Y.P. Lu, Intermetallics 72 (2016) 44–52 https://doi.org/10.1016/j.intermet.2016.01.008.
[42] P.H. Wu, N. Liu, P.J. Zhou, Z. Peng, W.D. Du, X.J. Wang, Y. Pan, Mater. Sci. Technol. 32 (2016) 576–580 https://doi.org/10.1179/1743284715Y.0000000127.
[43] W.L. Wang, L. Hu, S.B. Luo, L.J. Meng, D.L. Geng, B. Wei, Intermetallics 77 (2016) 41–45 https://doi.org/10.1016/j.intermet.2016.07.003.
[44] T. Guo, J. Li, J. Wang, Y. Wang, H. Kou, S. Niu, Intermetallics 86 (2017) 110–115 https://doi.org/10.1016/j.intermet.2017.03.021.
[45] Z. Peng, N. Liu, S.Y. Zhang, P.H. Wu, X.J. Wang, Mater. Sci. Technol. 33 (2017) 1352–1359 https://doi.org/10.1080/02670836.2017.1290736.
[46] A. Munitz, M.J. Kaufman, R. Abbaschian, Intermetallics 86 (2017) 59–72 https://doi.org/10.1016/j.intermet.2017.03.015.
[47] S. Wang, Z. Chen, L.C. Feng, Y.Y. Liu, P. Zhang, Y.Z. Hea, Q.Q. Menga, J.Y. Zhanga, Mater. Charact. 144 (2018) 516–521 https://doi.org/10.1016/j.matchar.2018.08.008.
[48] T. Nagase, Mater. Sci. Forum 941 (2018) 1238–1241 https://doi.org/10.4028/www.scientific.net/MSF.941.1238.
[49] A. Munitz, I. Edry, E. Brosh, N. Derimow, B.E. MacDonald, E.J. Lavernia, R. Abbaschian, Intermetallics 112 (2019) 106 517 https://doi.org/10.1016/j.intermet.2019.106517 .
[50] N. Derimow, R. Abbaschian, Entropy 20 (2018) 890 https://doi.org/10.3390/e20110890.
[51] S.H. Whang, J. Mater. Sci. 21 (1986) 2224–2238 https://doi.org/10.1007/BF01114261.
[52] S.A. Court, J.W. Sears, M.H. Loretto, H.L. Fraser, Mater. Sci. Eng. 98 (1988) 243–249 https://doi.org/10.1016/0025-5416(88)90,163-2.
[53] T. Nagase, M. Matsumoto, Y. Fujii, J. Alloys Compd. 738 (2018) 440–447 https://doi.org/10.1016/j.jallcom.2017.12.138.
[54] T. Nagase, M. Matsumoto, Y. Fujii, Microscopy 66 (S1) (2017) i22 https://doi.org/10.1093/jmicro/dfx064.
[55] A. Jain, S.P. Ong, G. Hautier, W. Chen, W.D. Richards, S. Dacek, S. Cholia, D. Gunter, D. Skinner, G. Ceder, K.A. Persson, APL Mater. 1 (1) (2013) 011002 https://doi.org/10.1063/1.4812323.
[56] https://materialsproject.org/ (accessed, 23 August 2019)
[57] T. Nagase, M. Suzuki, T. Tanaka, J. Alloys Compd. 619 (2015) 267–274 http://dx.doi.org/10.1016/j.jallcom.2014.08.229.
[58] T. Nagase, M. Suzuki, T. Tanaka, Intermetallics 61 (2015) 56–65 http://dx.doi.org/10.1016/j.intermet.2015.02.006.
[59] T. Nagase, M. Suzuki, T. Tanaka, J. Soc. Mater. Sci. 64 (2015) 175–182 http://dx.doi.org/10.2472/jsms.64.175.
[60] T. Nagase, M. Suzuki, T. Tanaka, J. Alloys Compd. 619 (2015) 311–318 http://dx.doi.org/10.1016/j.jallcom.2014.08.212.
[61] T. Nagase, Y. Umakoshi, J. Alloys Compd. 649 (2015) 1174–1181 http://dx.doi.org/10.1016/j.jallcom.2015.07.229.
[62] T. Nagase, M. Takemura, M. Matsumuro, M. Matsumoto, Y. Fujii, Mater. Des. 117 (2017) 338–345 http://dx.doi.org/10.1016/j.matdes.2016.12.092.
[63] T. Nagase, T. Terai, T. Kakeshita, M. Matsumoto, Y. Fujii, Mater. Trans. 60 (2019) 554–560 https://doi.org/10.2320/matertrans.Y-M2019803.
[64] A. Takeuchi, A. Inoue, Mater. Trans. 46 (2005) 2817–2829 https://doi.org/10.2320/matertrans.46.2817.
[65] Materials Project, HfZr, ID: mp-983,459, https://doi.org/10.17188/1316509
[66] T. Nagase, K. Mizuuchi, T. Nakano, Entropy 21 (2019) 483 https://doi.org/10.3390/e21050483.
[67] T. Nagase, M. Takemura, M. Matsumuro, T. Maruyama, Mater. Trans. 59 (2018) 255–264 (2018) http://doi.org/10.2320/matertrans.F-M2017851 .
[68] T. Nagase, T. Kakeshita, K. Matsumura, K. Nakazawa, S. Furuya, N. Ozoe, K. Yoshino, Mater. Des. 184 (2019) 108172 172 (2019) https://doi.org/10.1016/j.matdes.2019.108172 .
[69] Materials Project, Ti, ID: mp-72, https://doi.org/10.17188/1287108
[70] Materials Project, Zr, ID: mp-131, https://doi.org/10.17188/1189385
[71] Materials Project, Y, ID: mp-983,459, https://doi.org/10.17188/1187627
[72] G. Qin, R. Chen, P.K. Liaw, Y. Gao, L. Wang, Y. Su, H. Ding, J. Guo, X. Li, Nanoscale 12 (2020) 3965–3976 https://doi.org/10.1039/C9NR08338C.
[73] G. Qin, R. Chen, P.K. Liaw, Y. Gao, X. Li, H. Zheng, L. Wang, Y. Su, J. Guo, H. Fu, Scr.. Mater. 172 (2019) 51–55 https://doi.org/10.1016/j.scriptamat.2019.07.008.